Chapter

# Optical Phase-Modulation Techniques

*Ramón José Pérez Menéndez*

## Abstract

Optical phase-modulation technique is a very powerful tool used in a wide variety of high performance photonic systems. Fiber-optic sensors and gyroscopes, integrated-optics sensors, or high-performance photonic integrated circuits are some examples of photonic systems where the optical phase-modulation technique can be efficiently applied. In time, such a photonic system can be integrated as the core part of some specific applications like biosensors, 5G advanced optical communication devices, gyroscopes, or high-performance computation devices. In this work, the main optical phase-modulation techniques are analyzed. Also, a study of the most significant applications of this technique is made, relating it to the most appropriate type in each case.

**Keywords:** optical phase-modulation, electro-optic phase modulators, sinusoidal phase-modulation, square-wave phase-modulation, triangular phase-modulation, serrodyne phase-modulation, phase-locking technique, phase-locked-loop, optical gyroscopes

## 1. Introduction

Optical interferometry constitutes an important technique used in a high number of measurement processes for multiple physical magnitudes and quantitative phenomenon [1]. Particularly, fiber-optic waveguides can act as very useful and efficient transmission medium for light guidance in a large group of interferometry-based sensor devices. On the other hand, the study of subject of interferometer fiber-optic sensors has received an extensive treatment in the literature [2, 3]. In this article, a wide analysis of optical phase-modulation is made focused on the optical gyroscopes as the main referenced application. A simple open-loop configuration of interferometric fiber-optic gyroscope based on the Sagnac effect is shown in **Figure 1**. This kind of gyro is based on the Sagnac-effect within an open optical path realized by a N-turn fiber-optic coil when two independent counter-propagating light modes are externally introduced from a broadband laser source through its two ends, respectively. This causes that an interference pattern between the CW and CCW light beams to be collected in a photo-detector with a phase shift given by the following equation, Ref. [4]:

$$\phi_S = \frac{2\pi L D}{\lambda_0 c_0} \Omega \tag{1}$$

where $L$ and $D$ are length and diameter of fiber-optic sensing coil, respectively, $\lambda_0$ and $c_0$ are wavelength and speed of light source in vacuum, respectively, and $\Omega$ is the rotation rate. **Figure 1** clearly shows that this Interferometer-Fiber-Optic-Gyro (IFOG) has a passive configuration because the laser source is located externally to the sensing coil. In this system, the two counter-propagating light beams travel through the core of a conventional single-mode optical fiber (SMF) by total-internal-reflection phenomenon. As the core diameter of such an optical fiber is only about 8 μm, the spot size of the interference signal can only be coupled to a small area at the end of the fiber loop, for example on the small detection area of a photo-detector. So that, this interference signal affects only one or two interference fringes whose intensity can be evaluated by the following expression:

$$I(\phi) = I_0(1 + \cos\phi) \tag{2}$$

being $I(\phi)$ the output optical signal of interferometer, $I_0$ the amplitude of each of two CW and CCW counter-propagating beams and $\phi$ the optical phase-difference between them.

**Figure 2** represents the variation of light intensity along a single interference fringe as a function of $\phi$. Notice the output intensity noise produced when the phase difference is detected with a phase error $\Delta\phi$. Phase noise sources of this gyro, their influence on output signal and solutions are exhaustively treated in Refs. [5–16].

However, the simple and raw gyro configuration (laser-source, beam-splitter, fiber-coil sensor and photo-detector) showed in **Figure 1** is not effective in practice mainly due to its inability to reduce phase errors. Thus, the decrease in phase error can be effectively achieved by a phase-modulation process of CW and CCW optical

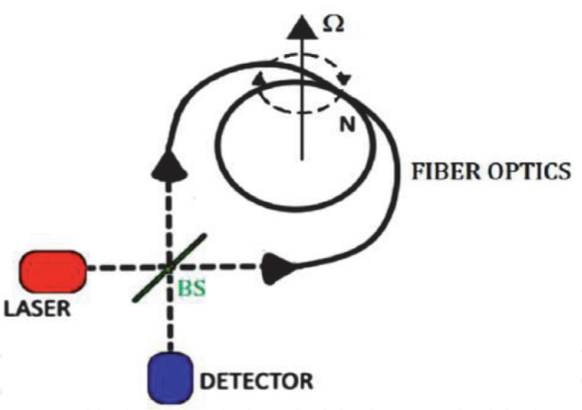


**Figure 1.**
*Basic structure of the IFOG.*

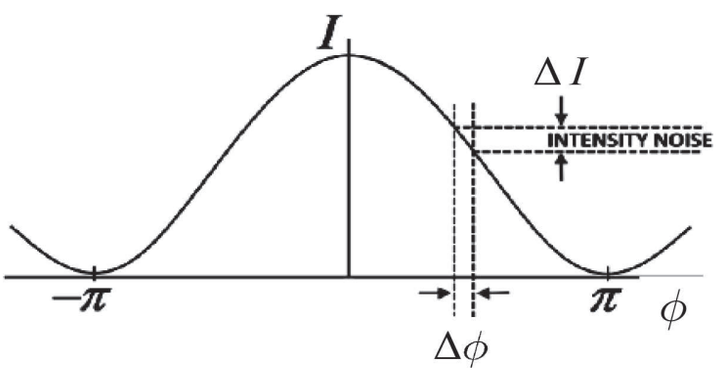


**Figure 2.**
*Two-beam interference response curve as a function of ϕ (phase-difference).*

waves by adding an optical phase-modulator in the path of the waves entering the optical fiber sensing coil as it is shown in the arrangement of **Figure 3**. Phase error decreasing is mainly achieved by electronic filtering within phase-sensitive demodulation circuits (PSD).

In this scheme, the immediate consequence of the application of a phase modulation to CW and CCW waves is the need to have an electronic demodulation system for the optical phase (commonly called PSD). This electronic phase-sensitive demodulation system must be located at the electric output of photo-detector. This way, by a demodulation process of electrical output signal of photo-detector, the Sagnac phase shift can be retrieved as calculated from Eq. (1) when a rotation-rate Ω is applied to the whole system. Also, as showed in **Figure 3**, other elements like a second beam splitter, a polarizer and an optical filter are needed to complete the system. The main function of the electro-optical phase modulator is to provide a controlled phase shift which will be added to Sagnac phase shift produced by the rotation onto the system. This way, the signal detected by photo-detector can be demodulated with some ease to recover by electronic means the Ω rotation-rate value which affects the whole system.

A more advanced design is achieved by closing the measurement loop by means of a feedback signal becoming into the scheme so-called IFOG closed loop configuration. The general scheme of a closed loop IFOG is depicted on **Figure 4**. In this scheme, the output signal of demodulator circuit passes through a servo amplifier

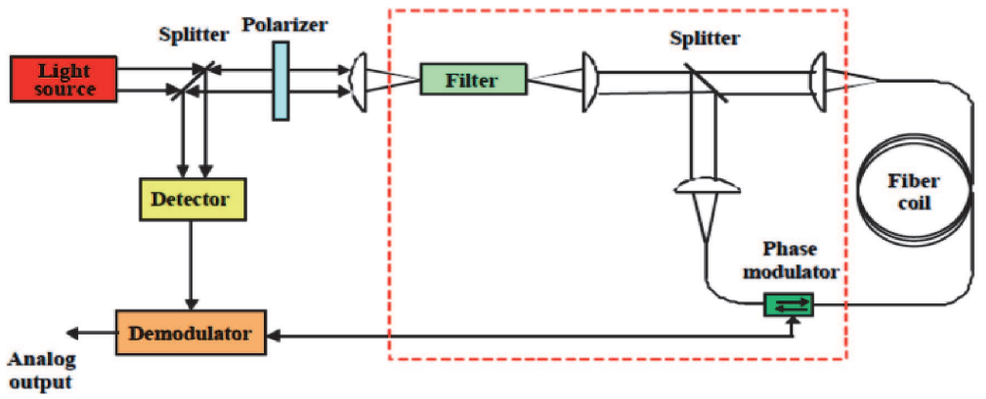


**Figure 3.**
*Complete bulk-optics fiber-optic gyro open-loop configuration.*

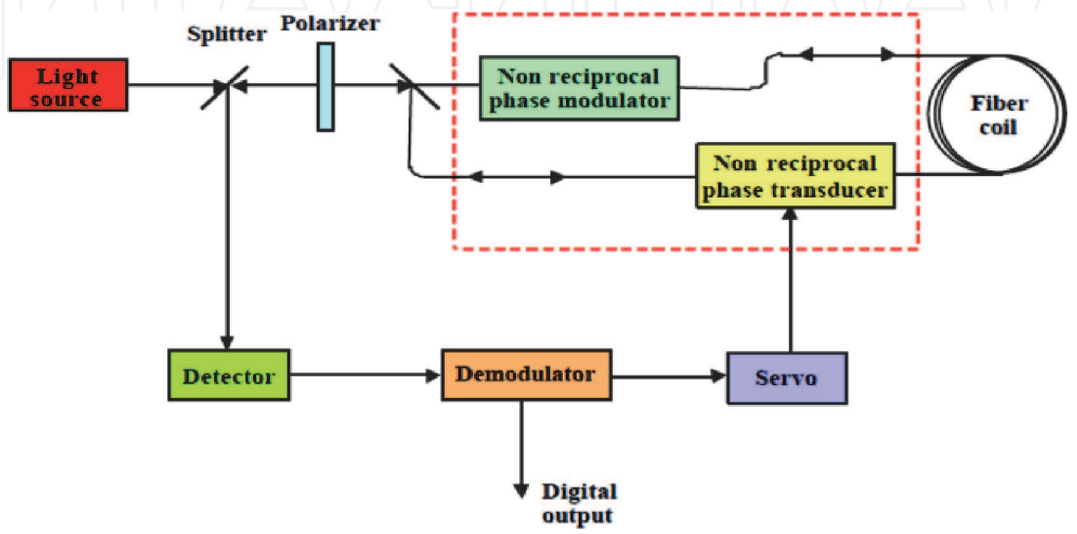


**Figure 4.**
*Typical closed-loop IFOG configuration.*

which drives a phase transducer placed in the interferometer path. Then, the whole system works under the phase-nulling principle. This means that the total phase shift becomes equal to zero because the phase transducer introduces a non-reciprocal phase shift that is equal, by in the opposite sign, to that generated by Sagnac phase shift induced by rotation. The output of the system is then the output of the phase transducer.

The main advantage of this configuration is the insensitivity to the laser source amplitude variations and the electronic circuitry gain because the system is always operated at zero total phase shift. Other design alternatives are possible, and so instead of using a fiber optic coil as a sensor it can be used a ring resonator integrated in a silicon waveguide, Ref. [17].

For open-loop configuration square-wave bias and sinusoidal phase modulation are usually applied while for closed-loop configuration, sinusoidal or square-wave bias and serrodyne feedback phase modulations are frequently used. In the following, a particular study of all these types of optical phase modulation will be made.

## 2. Square-wave optical phase modulation

One of the first attempts to apply the principle of phase modulation to CW-CCW optical waves in an optical gyroscope can be seen in Ref. [18]. In this case, a sinusoidal-wave phase modulation is applied mainly due first to the ease of finding fast bulk phase modulators in lithium niobate ($LiNbO_3$), Ref. [19], and also reliable electronic sine wave oscillators. However, square-wave is frequently used as bias phase modulation because it allows periodically shift the working point of the gyro to each one of $\pm\pi/2$ constant values, respectively. This last is due that when the central working point of the gyro is either $+\pi/2$ or $-\pi/2$, its sensitivity reach a maximum value, as it can be seen on **Figure 5**. Then, when the system is not subjected to rotation ($\Omega = 0$), the output response is a pectinate-shaped curve with a constant value. But, when the system is subjected to a non-zero rotation rate, the interferometric response output curve is also a Square-Wave whose peak-to-peak amplitude is proportional to the value of the rotation speed. The latter can also be also checked by observing in detail the **Figure 6**. In this figure, $\tau$ is the transit time of the CW and CCW optical waves over the fiber-coil length and $\phi_S$ is the Sagnac phase shift caused between them by rotation.

For this purpose, one phase modulator is located at the end of fiber coil, as represented in the scheme of **Figure 4**. Thus, the calculation of effective phase shift induced by the phase modulation process between CW and CCW optical waves at the output of fiber coil after their respective roundtrip can be expressed as follows:

$$\Delta\phi(t) \;=\; \phi_{CCW}(t) - \phi_{CW}(t) = \phi(t) - \phi(t-\tau) \tag{3}$$

In Eq. (3), $\phi(t)$ represents the time waveform of applied phase modulation and $\tau$ is, again, the transit time around the fiber coil which, in time, can be calculated as:

$$\tau \;=\; \frac{nL}{c} \tag{4}$$

here, $n$ is the effective refractive index of fiber, $L$ is the total length of fiber coil and $c$ is the vacuum speed of light. For obtaining the result of Eq. (3) it has been taken into account that CW and CCW waves enter the fiber coil at opposite ends. Then, in the case of square-wave phase modulation as represented in **Figure 6**,

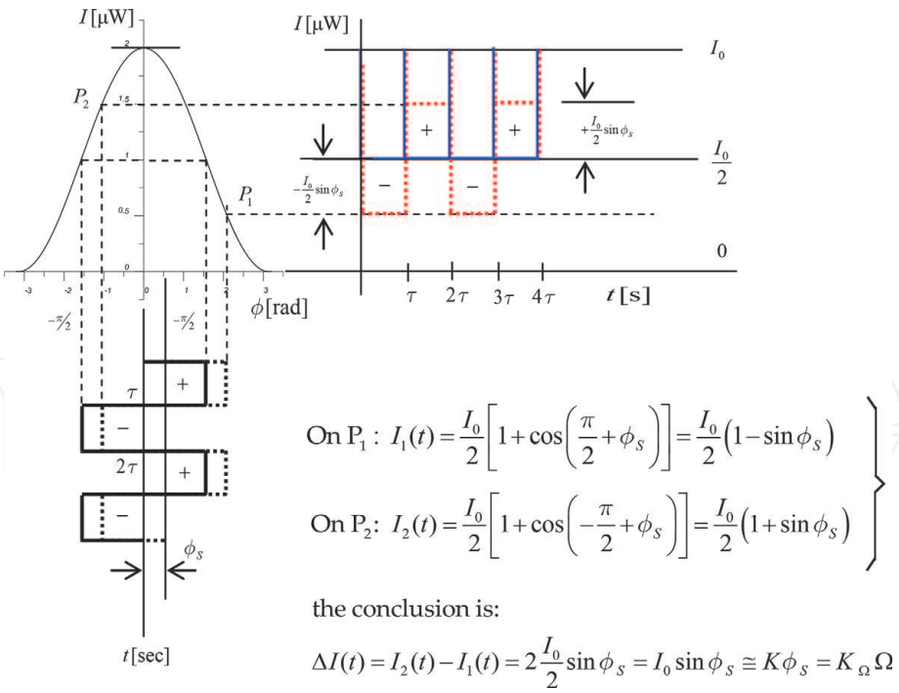


**Figure 5.**
*Analysis of the interference response of the gyro with square-wave phase modulation (solid blue curve: zero rotation, dotted red curve: non-zero rotation).*

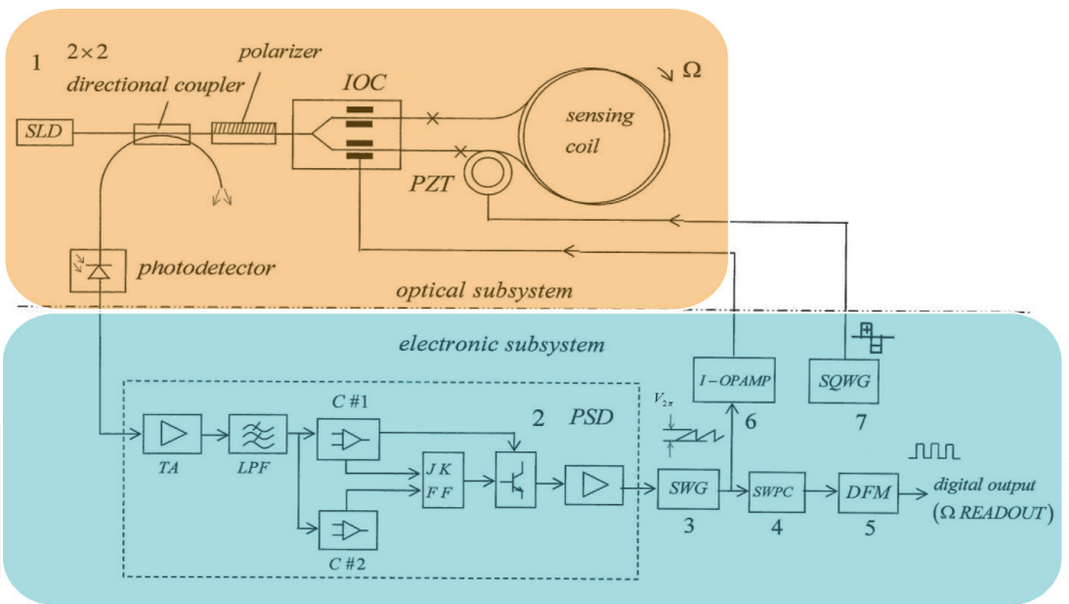


**1- Optical Subsystem**
**2- Phase-Sensitive-Demodulator (PSD)**
**3- Sawtooth-Wave-Generator (SWG)**
**4- Sawtooth-Wave-to-Pulse-Converter (SWPC)**
**5- Digital-Frequency-Meter (DFM)**
**6- Inverter-Operational- Amplifier (I-OPAMP)**
**7- Square-Wave-Generator (SQWG)**

**Figure 6.**
*Closed-loop IFOG scheme with square-wave BIAS and serrodyne FEEDBACK phase modulations (below, in the inset, the block-diagram definition).*

analytics gives two constant phase values, namely, $\pm\pi/2$ (continuous black wave) when no-rotation is applied to the system. However, when a non-zero rotation is applied, a phase difference equal to $\phi_S$ Sagnac phase shift must be added to phase

difference applied by the external phase modulation process. The explanation of blue (continuous) and red (dotted) output response curves of photo-detector is as follows. When rotation rate is equal to zero, the projection of the points of the input square waveform (continuous black) on the response curve of the interferometer gets a pectinate-shaped output waveform (continuous blue curve). However, when a non-zero rotation rate, a pectinate square-wave is obtained (dotted red curve). In this last case, as seen in the inset of **Figure 6**, the peak-to-peak square-wave value is very close proportional to rotation rate and can be evaluated as:

$$\Delta I(t) \;=\; I_0 \sin\phi_S \;\cong\; K\phi_S \;=\; K_\Omega\,\Omega \tag{5}$$

where the approximation can be justified because the value of the sine-function can be approximated by its argument when it is less than π/6 in absolute value.

**Figure 6** shows a closed-loop block-diagram scheme of an IFOG model with square-wave BIAS and serrodyne FEEDBACK phase modulations. In this case it is necessary to use two different phase modulators, first one to apply the square wave BIAS and second one for the serrodyne FEEDBACK phase modulation. See the complete description of this block-diagram on Ref. [20].

Gyro designs with square-wave kind of phase modulation can be seen in Refs. [21–24]. Last three engineered by Chinese authors utilize square waves staggered by sections (four-, five- or six-points phase modulation, respectively) and their main advantage is that all these schemes allow to improve the accuracy and scale factor of the gyro.

## 3. Sinusoidal optical phase modulation

The basic idea to apply the sinusoidal bias phase modulation to an IFOG configuration is that the amplitude of the first harmonic component of interferometer output signal contains information of the $\phi_S$ Sagnac phase shift induced by rotation. In particular, this amplitude can be considered approximately linearly proportional to the absolute value of rotation rate that affects the system. This fact will be analytically derived next. Suppose first a simple open-loop IFOG configuration, like that represented on **Figure 3**. Then, a sinusoidal bias phase modulation is applied to phase modulator, like the supplied by an electric sine oscillator working at $f_m$ frequency and amplitude $\phi_0$ in the following form:

$$\phi_m(t) \;=\; \phi_0\,\sin(\omega_m t) \tag{6}$$

The phase difference between CW and CCW waves induced by this bias phase modulation will be:

$$\begin{aligned}
\Delta\phi_m(t) \;&=\; \phi_{CCW}(t) - \phi_{CW}(t) = \phi_m(t) - \phi_m(t-\tau) \\
\Delta\phi_m(t) \;&=\; 2\phi_0\,\sin\left(\frac{\omega_m\,\tau}{2}\right)\cos\left[\omega_m\left(t-\frac{\tau}{2}\right)\right] \\
&\xrightarrow{\omega_m\,\tau=\pi}\; 2\phi_0\,\cos\left[\omega_m\left(t-\frac{\tau}{2}\right)\right] = \phi_m\,\sin(\omega_m t)
\end{aligned} \tag{7}$$

here $2\phi_0 = \phi_m$. As it can be seen from this equation, the maximum value of phase difference modulation for a given value of $\phi_0$ amplitude will be reached when the $\omega_m\tau = \pi$ condition to be accomplished. This condition is reached when the frequency $f_m$ equals the value:

$$f_m = \frac{1}{2\tau} \tag{8}$$

referred as proper frequency of the system, here $\tau$, the transit time. Then, under these conditions, when a rotation with $\phi_S$ Sagnac phase shift affects the system, the total phase difference between CW and CCW waves will be:

$$\Delta\phi(t) \;=\; \Delta\phi_m(t) + \phi_S = \phi_m \,\sin\,(\omega_m t) + \phi_S \tag{9}$$

Therefore, the interference signal can be obtained by the following calculation:

$$\begin{aligned} I(\Delta\phi) &= I_0[1 + \cos\,(\Delta\phi)] = I_0[1 + \cos\,[\phi_m \,\sin\,(\omega_m t) + \phi_S]] \\ &= I_0 \left\{ \begin{array}{l} 1 + \left[ J_0(\phi_m) + 2\sum_0^\infty J_{2n}(\phi_m)\,\cos\,(2n\,\omega_m t) \right] \cos\,(\phi_S) \\ -2\sum_0^\infty J_{2n-1}(\phi_m)\,\sin\,[(2n-1)(\omega_m t)]\,\sin\,(\phi_S) \end{array} \right\} \end{aligned} \tag{10}$$

here $J_n$ is the Bessel function of first kind and n-order. From Eq. (10) it can be observed that interference signal is the sum of three terms: a constant first term that does not depend on the frequency of modulation, a second term that includes the factor $\cos\,(\phi_S)$ multiplied by one infinite sum of even harmonics and a third term that includes the factor $\sin\,(\phi_S)$ multiplied by one infinite sum of odd harmonics. When $\phi_m$ value is adjusted to be 1.84, then the $J_1$ term reach its maximum value, namely, $J_1(1.84) = 0.5815$. It has also been shown that the amplitude of higher-order odd harmonics (3rd, 5th and successive) are getting smaller and smaller so their contribution can be neglected. Therefore, when a rotation rate affects the system, an electronic selective filtering of odd harmonics of interference signal is convenient to isolate and extract the data of rotation speed. Particularly, the first harmonic is the most convenient to recover, so that an electronic band-pass filtering at fundamental frequency of modulation should be added as phase-sensitive demodulator. This way, a successive low-pass filtering located after the band-pass one could retrieve the first harmonic amplitude, which is proportional to $\phi_S$ Sagnac phase shift and, in turn, to rotation rate value.

**Figure 7** represents the analytic sinusoidal phase modulation process. As it can be seen, when no rotation is applied, the interference signal (solid, blue curve) also contains even harmonics since the $\sin\,(\phi_S)$ factor is canceled. However, when rotation is applied, both even and odd harmonics appear (dotted, red curve) in the interference output signal since the $\sin\,(\phi_S)$ and $\cos\,(\phi_S)$ are not canceled.

**Figure 8** represents the block-diagram of a closed-loop IFOG configuration with sinusoidal BIAS and serrodyne FEED-BACK phase modulations, see Ref. [30]. The main novelty of this design is the structure of phase modulation feedback chain. In this case, one FET transistor (2N3848) is added on feedback branch of integrator OPAMP (block #7 on **Figure 8**). This block generates a linear ramp voltage Vγ on its output, and this ramp resets each one time-period driving by $V_{gate}$ voltage. In this way, a resultant serrodyne-wave voltage is easily generated at the output of integrator circuit, obtaining finally the same intended sawtooth-wave voltage on feedback phase modulation chain as reported on previous designs. The output signal of the photodetector, in photocurrent form, is proportional to the light intensity at its optical input. This photocurrent signal is converted to voltage with a trans-impedance amplifier that is placed at the input of demodulation circuit. The demodulation circuit (PSD) takes the task of extracting the information of the $\phi_S$ Sagnac phase shift induced by rotation. The corresponding voltage signal at its

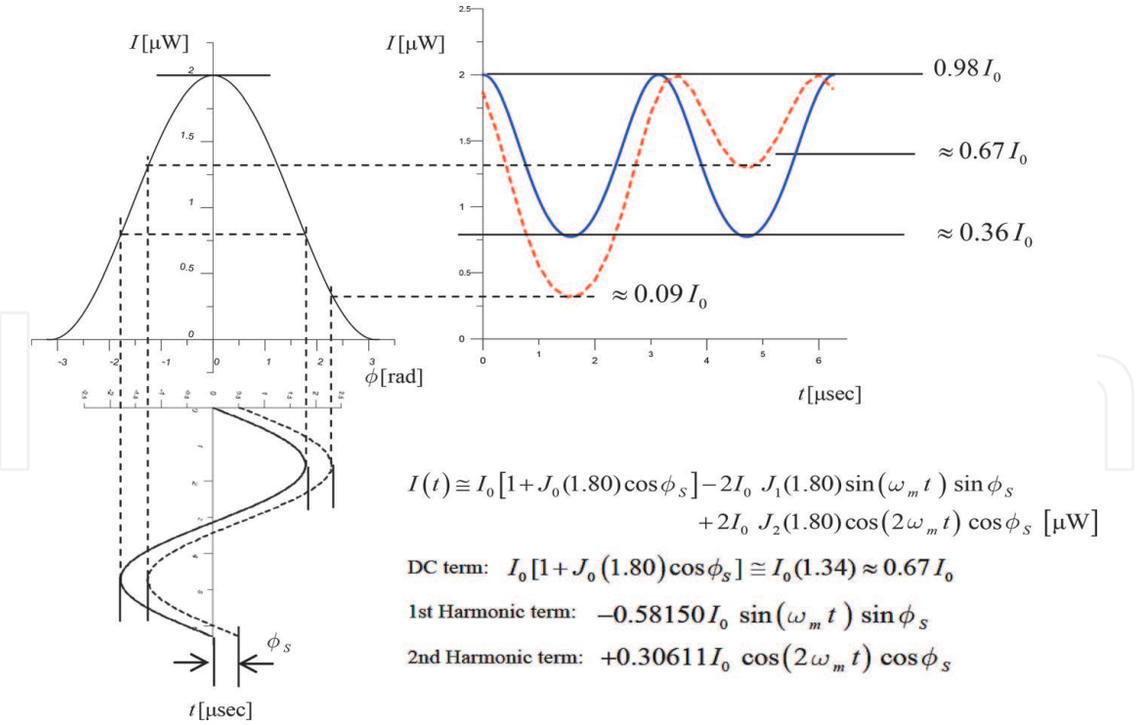


**Figure 7.**
*Analysis of the interference response of the gyro with sinusoidal phase modulation (solid blue curve: zero rotation, dotted red curve: non-zero rotation).*

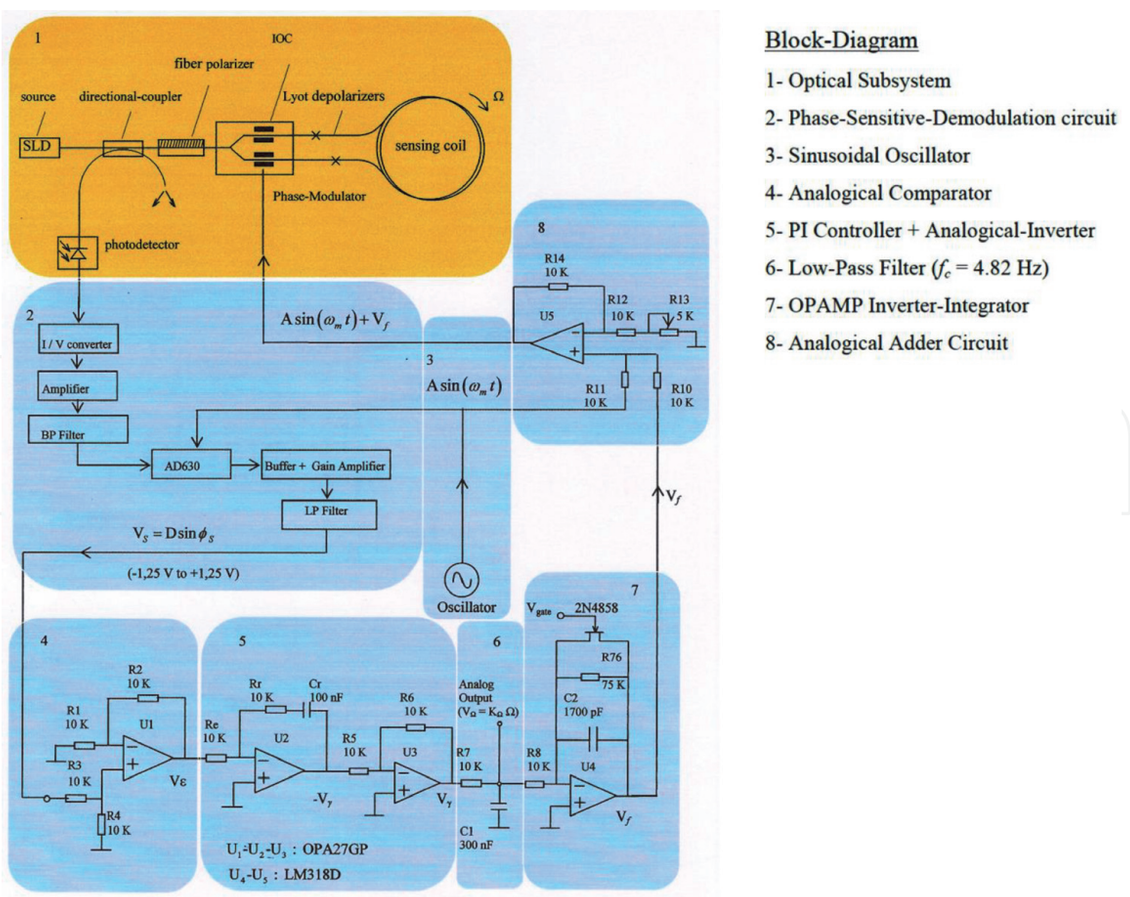


**Figure 8.**
*Closed-loop IFOG scheme with sinusoidal BIAS and serrodyne FEEDBACK phase modulations, see Ref. [30] (below, in the inset, the block-diagram definition).*

output ($V_S$) scales as sine-function of $\phi_S$. The PI controller realizes an integration of $V_S$ signal in time-domain, so that a voltage signal (Vγ) is obtained; this signal scales almost linearly with the time. This latter signal is filtered by means of a low-pass filter so that the corresponding output signal ($V_\Omega$) is a DC voltage value that is more accurately proportional to the gyroscope rotation-rate Ω (since the following approximation is fulfilled in the working range: $\sin\phi_S \approx \phi_S$). Therefore, the $V_\Omega$ analog output voltage signal constitutes the measurement of the rotation rate of the system. The control system, as a whole, acts as the principle of phase nulling. The phase-nulling process consists of generating a phase displacement ($\phi_m = \phi_{bias} + \phi_f$) in such a way that the $\phi_f$ phase-difference associated with the voltage output signal ($V_f$) is equal and with opposite sign with regard to the Sagnac phase-shift induced by the rotation rate, i.e., $\phi_f = -\phi_S$. To achieve this, the feedback phase modulation circuit holds a sample of the output signal $V_\Omega$. Note that this voltage signal is obtained at the end of low pass filter (Block #6 on **Figure 8**) and is proportional to rotation-rate Ω. An integration operation is needed for obtaining a linear ramp voltage to apply on phase modulator. Then, it integrates and inverts this signal by means of an operational integrator-inverter circuit, turning this signal into the following form:

$$V_f = -\frac{1}{RC}\int_0^t V_\Omega\, dt \tag{11}$$

This way, the time variation of $V_f$ voltage signal is a linear ramp, being its slope proportional to the rotation rate of the system ($V_\Omega$). **Figure 8** represents clearly the optical and electronic subsystems of the gyroscope, including the feedback phase-modulation and bias phase-modulation circuits for getting phase-nulling process, both applied together to PM (phase-modulator). Referring now to **Figure 8**, the total voltage signal applied to PM will be:

$$V_m = V_{bias} + V_f \tag{12}$$

Therefore, the output signal of the phase modulator will be the sum of the phase-difference signals associated with the $V_{bias}$ and $V_f$ voltages. In terms of phase differences, this is expressed as $\phi_m = \phi_{bias} + \phi_f$. Then, the error signal at the output of the comparator ($V\varepsilon$ voltage) tends to be nulled in average-time, due to the phase cancelation (since the average-time of the reference bias phase-modulation $\phi_{bias}$ is 0).

Sinusoidal phase modulation has been used on either open-loop (Refs. [18, 25, 26]) or closed-loop (Refs. [27–30]) IFOG configurations. In both cases, the PSD block (phase-sensitive-demodulation) must contain two selectively adjusted filtering circuits. First one is a low-pass filter with high enough cut-off frequency to filter the first harmonic component. Second one is a selective band-pass-filter to filter the component of first harmonic of interference signal, see also Ref. [30].

## 4. Serrodyne optical phase modulation

As announced at the beginning of this work, serrodyne-wave optical phase modulation is frequently used in closed loop IFOG schemes to configure one

feedback signal which is able to cancel the $\phi_S$ Sagnac phase shift induced by rotation. The justification for this is that the serrodyne-wave is the only one that produces a constant phase difference when applied to phase modulator (PM) in a gyro. This last

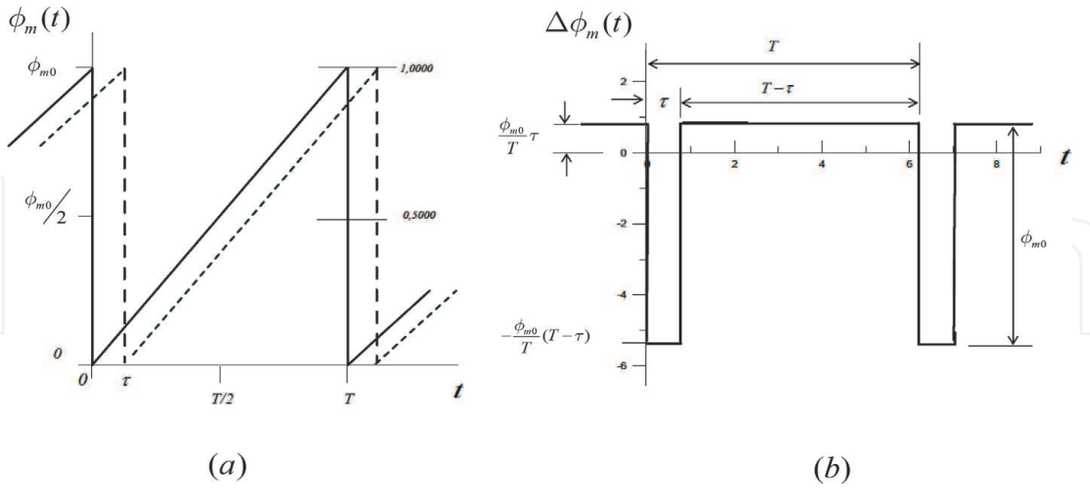


**Figure 9.**
*Serrodyne-wave phase modulation: (a) serrodyne-wave applied to PM with amplitude $\phi_{m0}$ and period T and (b) effective phase-difference $\Delta\phi_m(t)$as a function of time.*

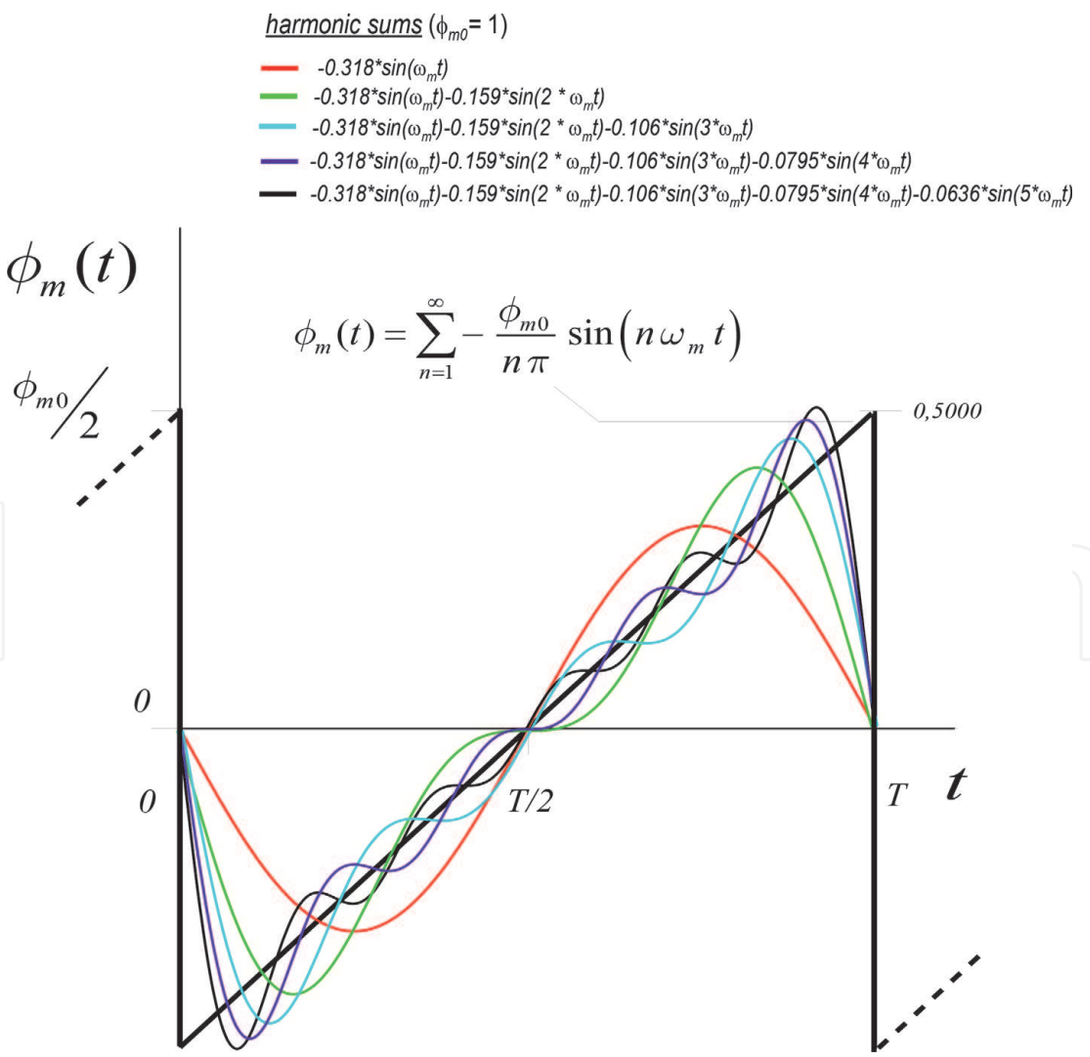


**Figure 10.**
*Fourier series development (Ref. [34]) of the sawtooth wave. In the upper inset, sum series contain the following: 1st harmonic (red curve); 1st and 2nd harmonics (blue curve); 1st, 2nd, and 3rd harmonics (green curve); 1st, 2nd, 3rd, and 4th harmonics (cyan curve); and finally, 1st, 2nd, 3rd, 4th, and 5th harmonics (black curve).*

can be checked observing the **Figure 9(b)**. During a time span equal to $(T - \tau)$ the phase-difference between CW and CCW waves remains constant with a value equal to $\frac{\phi_{m0}}{T}\,\tau$, being $\tau$ the transit time of light around the fiber coil. In addition, a constant value of 2 π is usually taken as the $\phi_{m0}$ amplitude of phase modulation in most part of designs. This way, by adjusting appropriately the period $T$ (or the frequency) of serrodyne-wave, the resulting value of phase-difference can be exactly matched with the $\phi_S$ Sagnac phase shift to achieve the phase cancelation by means of a specific feed-back circuit located on the way of feed-back signal, see for example Refs. [30–33].

For a proper operation of feedback circuit, it is essential that the falling edge (reset time) of sawtooth-wave be as fast as possible (ideally instantaneous), Ref. [31]. Since that serrodyne- (or sawtooth-) referred waveform is a periodic waveform that accomplishes Dirichlet conditions in the (0,$T$) interval, it is susceptible to be developed in a Fourier series (Ref. [34]) such as the one following next:

$$\phi_m(t) = \sum_{n=1}^{\infty} -\frac{\phi_{m0}}{n\pi}\,\sin\left(n\,\omega_m\,t\right) \tag{13}$$

This result shows that the series only contains sine terms because it refers to an odd function. On the other hand that result is very useful for filtering design purposes as it can be seen on simulated plots represented in **Figure 10**. Here, a successive sums containing the harmonics: first one (red-curve), the first and second ones (green-curve), the first, second and third ones (blue-curve), the first, second, third and fourth ones (cyan-curve) and finally the first, second, third, fourth and fifth ones (black-curve) are represented. The more terms are taken from the sum series, the better the approximation will be to the perfect sawtooth waveform.

In order to realize the serrodyne-wave phase modulation an Voltage-Controlled-Oscillator (VCO) circuit must be designed. The condition that this circuit must comply is:

$$\phi_S = \frac{V_{2\pi}}{T}\,\tau \tag{14}$$

so that the frequency $f = 1/T$ of serrodyne-wave should be adjusted depending on the value of the $\phi_S$ Sagnac phase shift, i.e., the more be $\phi_S$, the more will be the frequency of serrodyne and, then, the lower the value of its period $T$. Several circuits have been designed to meet this condition. One of these circuits has been represented in **Figure 11** and is described in Ref. [35]. Other VCO circuit for serrodyne-wave generation has already been explained above for FEED-BACK phase modulation, see **Figure 8** and related Ref. [30].

Although the serrodyne wave is the one that produces the best results for the feed-back phase modulation purpose, other similar waves have been also proposed. For example, symmetric triangular-wave represented in **Figure 12** can also perform the same function. Since it is an odd function, its development in Fourier series only contains the odd harmonics, then, it can be expressed in the following way:

$$\phi_m(t) = 4\,\phi_{m0}\sum_{n=1}^{\infty}\frac{\sin\left(\frac{n\pi}{2}\right)}{n^2\,\pi^2}\,\sin\left(\frac{n\pi t}{T/2}\right) \qquad n = 1,3,5,\ldots \tag{15}$$

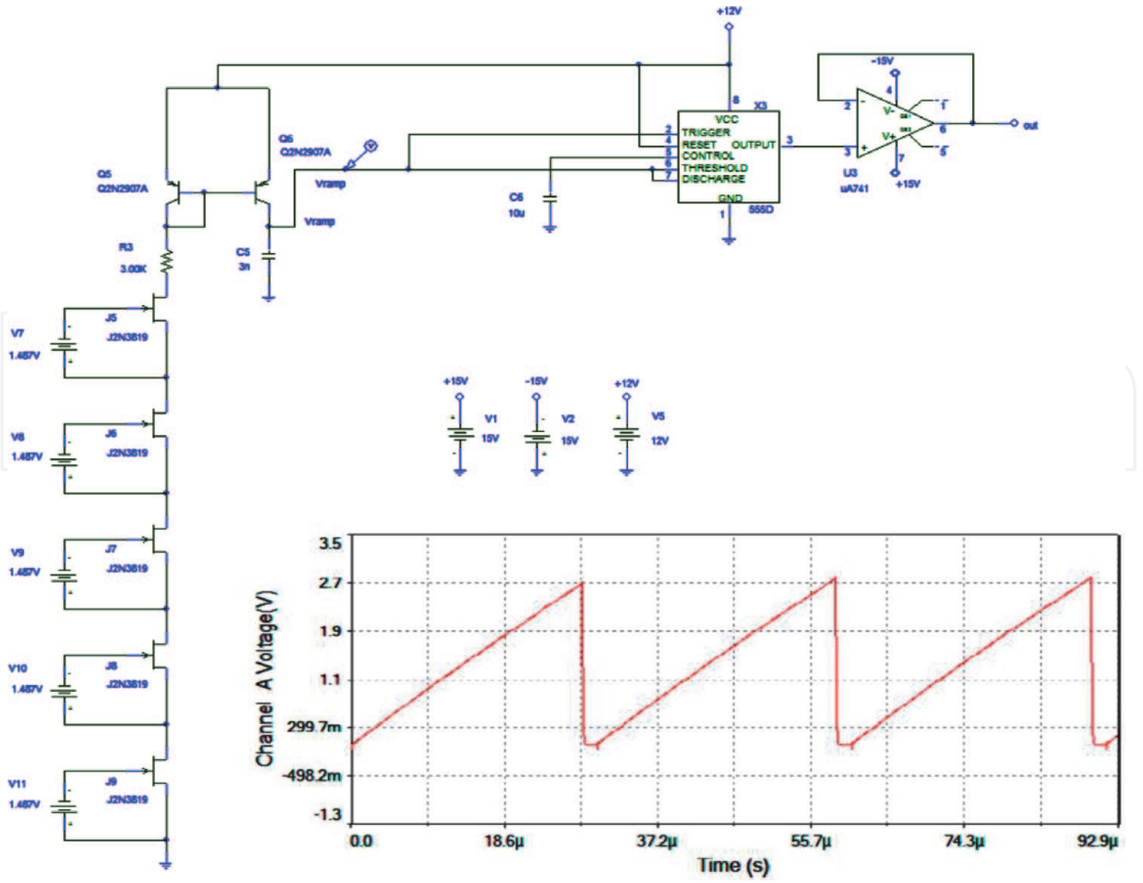


**Figure 11.**
*Serrodyne-wave VCO (voltage-controlled-oscillator) circuit with 555 IC (in the inset, 35.84 kHz linear ramp waveform generated), Ref. [35].*

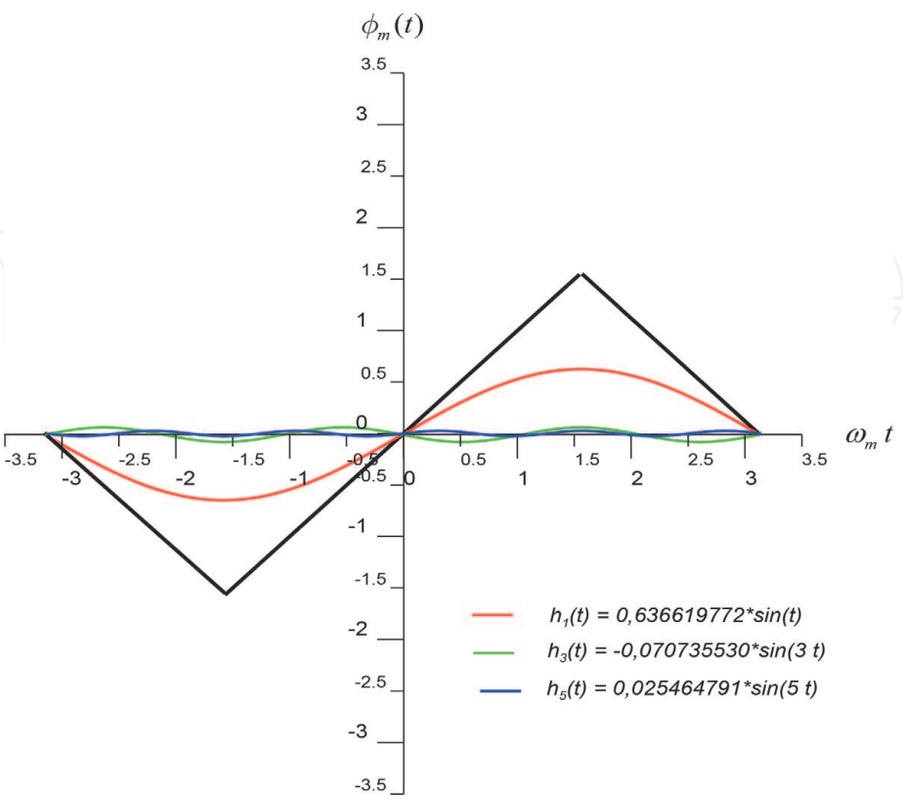


**Figure 12.**
*Symmetric triangular-wave with its 1st, 2nd and 3th harmonics, Ref. [35].*

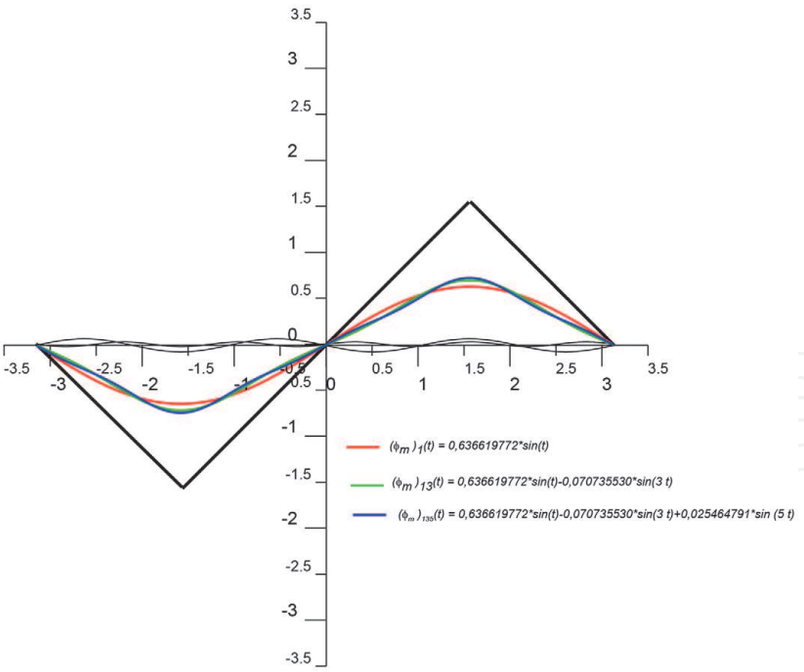


**Figure 13.**
*Symmetric triangular wave (in black) with its first three harmonic Fourier sums (red, green, blue), Ref. [34].*

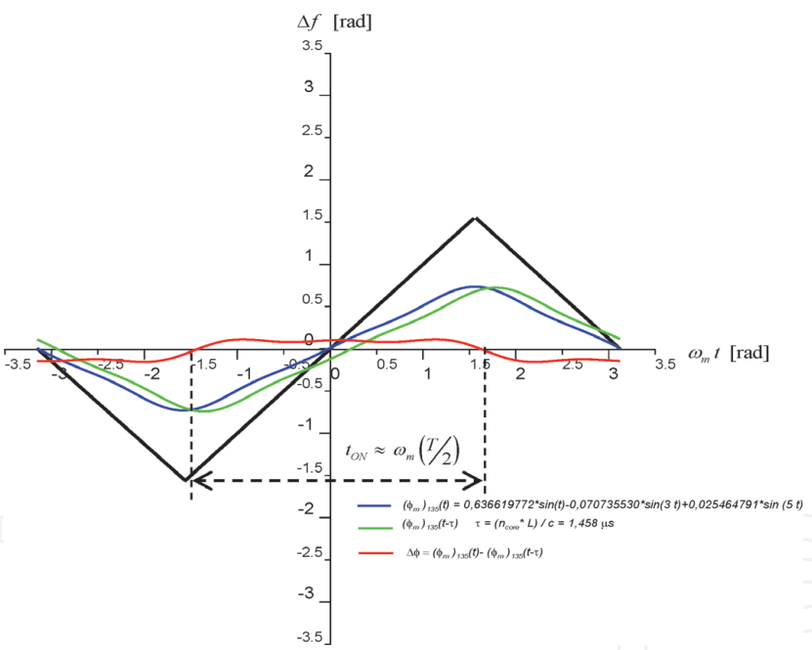


**Figure 14.**
*Effective phase-difference modulation of symmetric triangular wave (red-curve) related with its first three harmonic Fourier sums (blue, green) of CCW and CW optical waves, Ref [35].*

**Figure 13** represents the three first harmonic sums (red, green, blue) of symmetric triangular-wave (black). So that taking $\phi_{m0} = \pi/2$ in Eq. (15), the first three harmonic terms can be written as follows:

$$h_1(t) = \frac{4\phi_{m0}}{\pi^2}\sin\left(\frac{1\,\pi}{2}\right)\sin\left(\frac{\pi t}{T/2}\right) = 0,636619772\,\sin\left(t\right) \tag{16}$$

$$h_3(t) = \frac{4\phi_{m0}}{9\pi^2}\sin\left(\frac{3\pi}{2}\right)\sin\left(\frac{3\pi t}{T/2}\right) = -0,070735530\,\sin\left(3\,t\right) \tag{17}$$

$$h_5(t) = \frac{4\phi_{m0}}{9\pi^2} \sin\left(\frac{5\pi}{2}\right) \sin\left(\frac{5\pi t}{T/2}\right) = 0,025464791 \sin(5\ t) \tag{18}$$

This way, the first three harmonic Fourier sums can be expressed, respectively, as:

$$(\phi_m)_1(t) = \frac{4\phi_{m0}}{\pi^2} \sin\left(\frac{\pi t}{T/2}\right) \tag{19}$$

$$(\phi_m)_{13}(t) = \frac{4\phi_{m0}}{\pi^2}\left[\sin\left(\frac{\pi t}{T/2}\right) - \frac{1}{9}\sin\left(\frac{3\pi t}{T/2}\right)\right] \tag{20}$$

$$(\phi_m)_{135}(t) = \frac{4\phi_{m0}}{\pi^2}\left[\sin\left(\frac{\pi t}{T/2}\right) - \frac{1}{9}\sin\left(\frac{3\pi t}{T/2}\right) + \frac{1}{25}\sin\left(\frac{3\pi t}{T/2}\right)\right] \tag{21}$$

Then, the conclusion is that when the approximation of first three harmonic Fourier sum of symmetrical triangular-wave is taken in gyro phase modulation (blue and green curves in **Figure 14**), its effective phase-difference (red curve in **Figure 14**) can be computed. In this case, one switching circuit is needed.

## 5. Conclusions

Square, sinusoidal, serrodyne and symmetric triangular waveforms can be used in phase modulation processes for optical Sagnac interferometer gyros. For open-loop gyro schemes only one square-wave or sinusoid$$PM) to retrieve the Sagnac phase shift induced by rotation. However, for closed-loop scheme gyros two waveforms are needed, the first one (square-wave or sinusoidal-wave) for the bias phase modulation and the second one (serrodyne-wave or triangular-wave) for the feedback phase modulation aiming the phase cancellation (phase-nulling). In the closed-loop scheme, the output signal of the phase-sensitive-demodulator (PSD) circuit passes through a servo-amplifier which drives a phase-shifter transducer placed in the interferometer path. Then, the phase transducer introduces a non-reciprocal phase shift that is equal, by in the opposite sign, to Sagnac phase shift induced by rotation. Thus, the output of the system is the output of the phase transducer. Closed-loop gyro configuration is advantageous with regard the open-loop one because a better accuracy (sensitivity) and scale-factor stability of the gyro are achieved.

IntechOpen

## Author details

Ramón José Pérez Menéndez
UNED-Spain, Lugo, Spain

*Address all correspondence to: ramonjose.perez@lugo.uned.es

## References


[1] Hariharan P. Optical Interferometry. 2nd ed. Academic Press; 2003. pp. 1-8

[2] Sharma U, Wei X. Fiber optic interferometric devices. In: Kang JU, editor. Fiber Optic Sensing and Imaging. New York: Springer; 2013. pp. 29-53 [chapter 2]

[3] Yin S, Ruffin PB, Yu FTS, editors. Fiber Optic Sensors. 2nd ed. CRC Press; 2008. pp. 333-366

[4] Vali V, Shorthill RW. Fiber ring interferometer. Applied Optics. 1976; **15**(5):1099-2000

[5] Bohm K, Marten P, Petermann K, Weidel E, Ulrich R. Low-drift using a superluminescent diode. Electronics Letters. 1981;**17**:352-353

[6] Ruffin PB, Smith RH. Fiber winding approaches for environmentally robust IFOG sensor coils. SPIE of Proceedings, 1792. Components for Fiber Optic Applications. 1992. p. 179

[7] Bergh RA, Lefevre HC, Shaw HJ. All-single-mode fiber-optic gyroscope. Optics Letters. 1981;**6**(4):198-200

[8] Bergh RA, Lefevre HC, Shaw HJ. Compensation of the optical Kerr effect in fiber-optic gyroscopes. Optics Letters. 1982;**7**:282-284

[9] Bergh RA, Lefevre HC, Shaw HJ. Overview of fiber-optic gyroscopes. IEEE Journal of Lightwave Technology. 1984;**LT-2**:91-107

[10] Moeller RP, Burns WK, Frigo NJ. Open-loop output and scale factor stability in a fiber-optic gyroscope. Journal of Lightwave Technology. 1989; **7**(2):262-269

[11] Hotate K, Tabe K. Drift of an optical fiber gyroscope caused by the faraday effect: Influence of the earth's magnetic field. Applied Optics. 1986;**25**: 1086-1092

[12] Bohm K, Petermann K, Weidel E. Sensitivity of a fiber optic gyroscope to environmental magnetic fields. Optics Letters. 1982;**6**:180-182

[13] Bergh RA, Culshaw B, Cutler CC, Lefevre HC, Shaw HJ. Source statistics and the Kerr effect in fiber-optic gyroscopes. Optics Letters. 1982;**7**: 563-565

[14] Takiguchi K, Hotate K. Method to reduce the optical Kerr-effec-induced bias in an optical passive ring-resonator gyro. IEEE Photonics Technology Letters. 1992;**4**:2

[15] Shupe DM. Thermally induced nonreciprocity in the fiber-optic interferometer. Applied Optics. 1980; **19**(5):654-655

[16] Ruffin PB, Lofts CM, Sung CC, Page JL. Reduction of nonreciprocity in wound fiber optic interferometers. Optical Engineering. 1994;**33**(8): 2675-2679

[17] Lefevre HC, Bettini JP, Vatoux S, Papuchon M. Progress in optical fiber gyroscopes using integrated optics. In: NATO-AGARD Conference Proceedings, 383, 9A1, 9A-13. 1985

[18] Kim BY, Shaw HJ. Phase-reading all-fiber-optic gyroscope. Optics Letters. 1984;**9**(8):378-380

[19] Wooten L, Kissa KM, Yi-Yan A, Murphy EJ, Lafaw DA, Hallemeier PF, et al. A review of lithium niobate modulators for fiber-optic communications systems. IEEE Journal of Quantum Electronics. 2000;**6**(1):69-81

[20] Pérez Menéndez RJ. Optoelectronic design of a 2045 m coil, closed loop-

based, depolarized IFOG with square-wave bias and Sawtooth-wave feedback optical phase modulations: Parametric modelling, simulation and performance test. In: Yurish SY, editor. Book Series: Advances in Sensors: Reviews. Vol. 5. Barcelona, Spain: IFSA Publishing S.L.; 2018

[21] Kay CJ. Serrodyne modulator in a fibre-optic gyroscope. IEE Proceedings Journal—Optoelectronics. 1985;**132**(5): 259-264

[22] Li X, Zhang Y, Yu Q. Four-state modulation in fiber optic gyro. In: 2008 IEEE International Conference on Mechatronics and Automation; Takamatsu. 2008. pp. 189-192

[23] Li X, Zhang Y, Zhang C. Five points modulation in closed loop fiber optic gyroscope. In: 2009 5th International Conference on Wireless Communications, Networking and Mobile Computing. Beijing; 2009. pp. 1-3

[24] Zhang C, Zhang S, Pan X, Jin J. Six-state phase modulation for reduced crosstalk in a fiber optic gyroscope. Optics Express. 2018;**26**:10535-10549

[25] Emge SR, Bennett S, Dyott RB, Brunner J, Allen DE. Reduced minimum configuration fiber optic gyro for land navigation applications. Aerospace and Electronic Systems Magazine. IEEE; 1997;**16**:18-21

[26] Bennett SM, Emge S, Dyott RB. Fiber optic gyroscopes for vehicular use. In: Proceedings of Conference on Intelligent Transportation Systems. Boston, MA, USA; 1997. pp. 1053-1057

[27] Kim BY, Shaw HJ. Harmonic feedback approach to fiber gyroscope scale factor stabilization. In: Proceedings. 1st Conference. Optical Fiber Sensors. London; 1983. pp. 136-137

[28] Kim BY, Shaw HJ. Gated phase-modulation feedback approach to fiber-optic gyroscopes. Optics Lettters. 1984;**9**(6):263-265

[29] Kim BY, Shaw HJ. Gated phase-modulation feedback approach to fiber-optic gyroscopes with linearized scale factor. Optics Lettters. 1984;**9**(8): 375-377

[30] Pérez Menéndez RJ. Optoelectronic design of a closed-loop depolarized IFOG with sinusoidal phase modulation for intermediate grade applications. 2018. pp. 215-223. DOI: 10.5772/intechopen.72592

[31] Kay CJ et al. Serrodyne modulator in a fibre-optic gyroscope. IEEE Proceedings Journal. 1985;**132**(5):259-264

[32] Ebberg A et al. Closed-loop fiber-optic gyroscope with a Sawtooth phase-modulated feedback. Optics Letters. 1985;**10**(6):300-302

[33] Skalský M, Habránek Z, Fialka J. Efficient modulation and processing method for closed-loop fiber optic gyroscope with piezoelectric modulator. Sensors (MDPI). 2019;**19**(7):1710

[34] Abramovitz M, Stegun I. Handbook of Mathematical Functions: With Formulas, Graphs and Mathematical Tables. Dover Publications; 1972. p 805

[35] Pérez RJ. Development of prototypes of single-mode fiber-optic interferometric sensor with phase modulation techniques for the measurement of differential rotation [PhD thesis]. Universidad de Oviedo-Spain. 2016. pp. 299-305. Available from: http://digibuo.uniovi.es/dspace/handle/10651/40188